Quantum Hall effect in multilayered massless Dirac fermion systems with tilted cones

Naoya Tajima,[1,2] Takahiro Yamauchi,[1] Tatsuya Yamaguchi,[1] Masayuki Suda,[3] Yoshitaka Kawasugi,[2] Hiroshi M. Yamamoto,[2,3] Reizo Kato,[2] Yutaka Nishio,[1] and Koji Kajita[1]

[1]*Department of Physics, Toho University, Miyama 2-2-1, Funabashi-shi, Chiba 274-8510, Japan*

[2]*RIKEN, Hirosawa 2-1, Wako-shi, Saitama 351-0198, Japan*

[3]*Research Center of Integrative Molecular Systems (CIMoS), Institute for Molecular Science, Okazaki 444-8385, Japan*

(Received 1 May 2012; revised manuscript received 8 July 2013; published 27 August 2013)

A massless Dirac fermion ststem was realized in α-(BEDT-TTF)$_2$I$_3$ [BEDT-TTF=bis(ethylenedithio) tetrathiafulvalene] under high pressure. In contrast to graphene, this is the first bulk (multilayered) massless Dirac fermion material. Another important difference from graphene is that this system has highly tilted Dirac cones. In this case, conventional chiral symmetry is broken under a magnetic field. Here we experimentally addressed the following question: Is the Landau level structure of the system with tilted Dirac cones the same as that of graphene [conventional two-dimensional (2D) Dirac fermion system] under a magnetic field? The answer is yes. We succeeded in injecting holes into α-(BEDT-TTF)$_2$I$_3$ under high pressure. The detection of Shubnikov–de Haas oscillations whose phase was modified by Berry's phase π is direct evidence that this system is truly a 2D Dirac fermion system. In addition, we revealed the energy diagram of this device and characterized the multilayered quantum Hall effect.

DOI: 10.1103/PhysRevB.88.075315 PACS number(s): 73.43.Fj, 72.80.Le

I. INTRODUCTION

Since the massless Dirac fermion system was discovered in graphene,[1,2] Dirac particles in other materials, such as graphite,[3,4] bismuth,[5] Fe-based superconductors,[6] topological insulators,[7] and organic conductors,[8–15] have also fascinated physicists. Among them, the organic conductor α-(BEDT-TTF)$_2$I$_3$ (Ref. 16) [Fig. 1(a)] under high pressure belongs to a broad category of the two-dimensional (2D) massless Dirac fermion system. This material is the first bulk (multilayered) 2D zero-gap conductor with massless Dirac particles. Another significant feature different from graphene and other systems is that the Dirac cones are highly tilted, as shown in Fig. 1(b).[13–15]

One of the characteristic features of conventional 2D Dirac fermion systems is seen in the magnetic field normal to the 2D plane. In the magnetic field, the energy of Landau levels in a zero-gap structure is expressed as

$$E_{\mathrm{nLL}} = \pm\sqrt{2e\hbar v_{\mathrm{F}}^2|N||B|}, \qquad (1)$$

where v_{F} is the Fermi velocity, N is the Landau index, and B is the magnetic field strength. In contrast to conventional conductors, this energy depends on the square root of B and N. At zero energy (Dirac point), the zero-mode ($N = 0$) Landau level always appears.[17]

In the case of tilted Dirac cones, however, conventional chiral symmetry is broken in the magnetic field. Can Eq. (1) also describe the energy of Landau levels in multilayered and/or tilted Dirac cone systems? α-(BEDT-TTF)$_2$I$_3$ under high pressure offers an ideal testing ground to answer this question.

In α-(BEDT-TTF)$_2$I$_3$, the zero-mode Landau level including its spin splitting is detected on interlayer transport. The detection of other Landau levels, however, poses a challenge because the Fermi level is always located at the Dirac point. Moreover, the multilayered structure makes control of the Fermi level by the field-effect transistor (FET) method much more difficult than the case of graphene. Thus, neither Shubnikov–de Hass (SdH) oscillations nor the quantum Hall effect (QHE) have been observed in this system until now. Resolving those issues, however, should lead us to the answer to the above question. Furthermore, it will provide us with the physics based on the multilayered QHE.

In the present work, we made a breakthrough in the carrier injection to α-(BEDT-TTF)$_2$I$_3$ under high pressure and detected SdH oscillations and the QHE. Our idea is described in the following.

According to an investigation of the Hall effect in α-(BEDT-TTF)$_2$I$_3$, the carrier density at low temperature is only 10^8cm^{-2}/sheet.[10] Yet the carriers are not localized but mobile

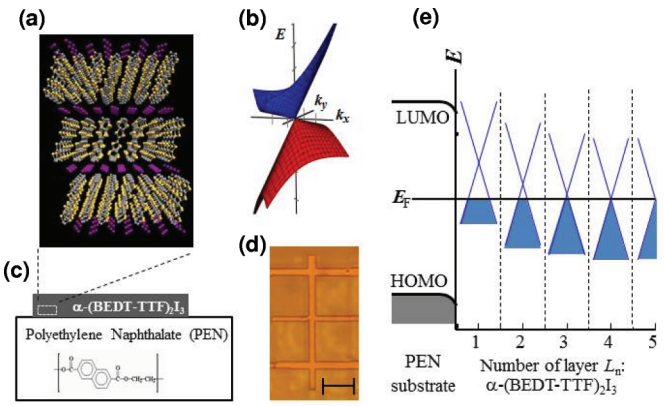

FIG. 1. (Color online) (a) Crystal structure of α-(BEDT-TTF)$_2$I$_3$ viewed from the a axis. (b) Band structure of α-(BEDT-TTF)$_2$I$_3$ under pressure. Note that the origins of the axes are taken at the position of the Dirac point. (c) Schematic diagram of this system. The thickness of the crystal measured with a step profiler was approximately 100 nm. (d) Optical image of a single crystal on a PEN substrate in the processed form. The crystal was cut by using a pulsed laser beam with a wavelength of 532 nm. The scale bar is approximately 0.2 mm. (e) Schematic energy diagram of the present device. The energy spectra (Dirac cones) for the layers are drawn.

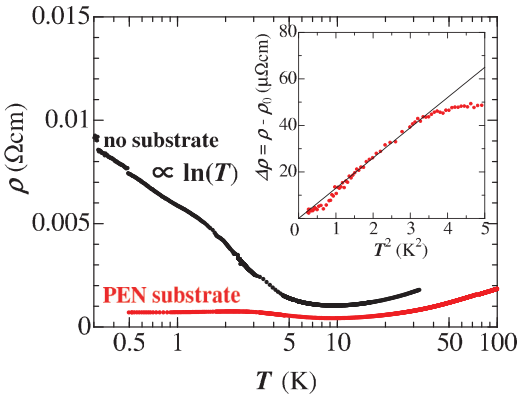

FIG. 2. (Color online) Temperature dependence of resistivity in multilayered Dirac fermion systems α-(BEDT-TTF)$_2$I$_3$ with PEN substrates. The inset shows $\Delta\rho = \rho - \rho_0$ against T^2, where ρ_0 is the resistivity at the limit of $T = 0$.

with high mobilities. Thus, by fixing a crystal onto a substrate weakly negatively charged by contact electrification, the effects of hole doping can be detected in the transport. Indeed, we detected the hole doping effects on the magnetoresistance and the Hall effect by fixing a crystal onto a polyethylene naphthalate (PEN) substrate [Fig. 1(b)]. Figure 1(e) is the prospective energy diagram of this device. Holes should be injected into a few layers (pairs of BEDT-TTF molecular layers and I_3^- anion layers; *vide infra*). From this study, we anticipate that the surface charge produced by contact electrification of the PEN substrate under high pressure is higher than 10^{-2} C m^{-2} at low temperatures.

Let us examine the characteristic transport in this device as follows. First, the effects of hole injection on the resistivity are briefly mentioned. Second, we report the observations of SdH oscillations and quantized Hall resistance in this device. In the discussion, we reveal the Landau level structure in the Dirac system with broken chiral symmetry and the energy diagram of this device. Moreover, the multilayered quantum Hall states are characterized.

II. METHODS

Single crystals of α-(BEDT-TTF)$_2$I$_3$ were synthesized by the electrolysis method. A crystal of approximately 100 nm thickness was tightly fixed onto a PEN substrate by van der Waals forces and/or electrostatic forces, as shown in Fig. 1(b). The resistivity and the Hall resistivity under the pressure of approximately 1.7 GPa were measured in magnetic fields of up to 7 T at 0.5 K. Experiments were conducted as follows. A sample to which eight electrical leads were attached was put in a Teflon capsule filled with a pressure medium (Idemitsu DN-oil 7373), and then the capsule was set in a clamp-type pressure cell made of BeCu hard alloy.

III. EXPERIMENTAL RESULTS

A. Resistivity of crystal with a PEN substrate

One of the effects is clearly seen in the resistivity. We show the temperature dependence of the resistivity in Fig. 2. First, the resistivity values of the crystal with the PEN substrate

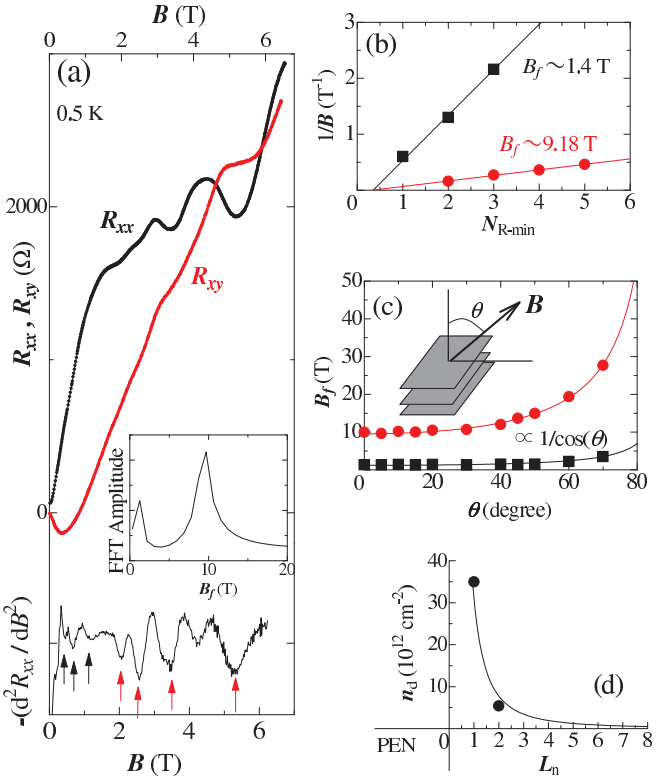

FIG. 3. (Color online) (a) Magnetic field dependence of R_{xx}, R_{xy}, and $-(d^2R_{xx}/dB^2)$ under the pressure of approximately 1.7 GPa. We find magnetoresistance oscillations with two frequencies at magnetic fields below 1.5 T (black arrows) and above 2 T (red arrows). We denote the oscillation $-(d^2R_{xx}/dB^2)$ minima by arrows. Note that the minimum at 4.2 T indicates spin splitting of the $N = -2$ Landau level. The inset shows the result of fast Fourier transform (FFT) analysis. On the other hand, the plateaus observed in R_{xy} at magnetic fields of approximately 3.5 and 5.5 T show that R_{xx} minima are the hallmarks of the QHE. (b) Value of B^{-1} for the SdH oscillation minima. In the case of Dirac fermion systems, the linear extrapolation of the data to $B^{-1} = 0$ should be $1/2$. For normal electrons, on the other hand, it is shifted to 0. (c) Angle dependence of B_f. (d) Distribution of doped carrier density in the layered direction. The line is the curve of $n(z) \propto (L_n + L)^{-2}$ with $L = 1$.

are lower than that of normal ones with no substrate. This strongly suggests that the carrier injection into a crystal is successful. The remarkable behavior is seen in the temperature region below 2 K. In the case of a crystal with no substrate, the resistivity obeys $\log T$ law.[12] This is also characteristic of the transport of Kondo-effect systems or the localized systems. However, we cannot explain this strong change in the resistivity in those pictures. It may be characteristic transport in this system at the vicinity of Dirac point.

On the contrary, the resistivity of the crystal with a PEN substrate, which is proportional to the square of temperature, strongly suggests that the Fermi liquid state is realized in this device. Thus, we succeeded in injecting carriers into α-(BEDT-TTF)$_2$I$_3$ with a layered structure, but the number of carrier doping layers was small, as shown in Fig. 1(e). Clearly, resistivity depends on crystal thickness.

B. SdH oscillations and quantized Hall resistance

Figure 3(a) shows the magnetic field dependence of resistance R_{xx} and Hall resistance R_{xy} under the pressure of approximately 1.7 GPa at 0.5 K. We notice an oscillation in R_{xx} at magnetic fields above 0.5 T. The fact that the resistance oscillates as a function of B^{-1} indicates that this is the SdH signal. Fourier analysis reveals two frequencies with $B_f = 1.4$ and 9.18 T, as shown in the inset of Fig. 3(a). The second-order differential of R_{xx} clearly depicts those oscillations, as indicated by arrows in Fig. 3(a), one with $B_f = 1.4$ T ($B < 1.5$ T) and another one with $B_f = 9.18$ T ($B > 2$ T).

On the other hand, the two obvious plateaus observed in R_{xy} at magnetic fields of approximately 3.5 and 5.5 T show that R_{xx} minima are the hallmarks of the QHE. We also find the anomalies at magnetic fields of approximately 2 and 2.5 T.

In what follows, we will discuss the Landau level structure, the energy diagram, and the quantum Hall states in this device from the quantum transport phenomena.

IV. DISCUSSIONS

A. Landau level structure in a Dirac fermion system with broken chiral symmetry

First, we demonstrate that both SdH oscillations in Fig. 3(a) originate from a 2D Dirac-type energy structure, as follows. In the case of a Dirac fermion system, the circular orbit around the Dirac point in the magnetic field would yield Berry's phase π. This phase would modify the Landau quantization condition so that the zero-mode ($N = 0$) Landau level would always appear at the Dirac point. The effect of this phase is further probed in the semiclassical magneto-oscillation description, such as SdH oscillations. The SdH oscillation part of resistivity written by

$$\Delta R_{xx} = A(B)\cos[2\pi(B_f/B + 1/2 + \gamma)] \qquad (2)$$

acquires the phase factor $\gamma = 0$ or $1/2$ for normal electrons with Berry's phase 0 and Dirac particles with Berry's phase π, respectively.[2] Here, $A(B)$ is the SdH oscillation amplitude. We obtain the phase factor γ by plotting the values of B^{-1} at the oscillation minima of ΔR_{xx} [Fig. 2(a)] as a function of their number, as shown in Fig. 3(b). The linear extrapolated values close to $1/2$ of the data to $B^{-1} = 0$ determine the phase factors γ, both of which are approximately $1/2$. Thus, we identify the Dirac particles. In the present devices, the carriers are injected into more than two layers, as shown in Fig. 1(e), and two layers from an interface emit SdH oscillations with different frequencies, respectively. As each layer is independent, the angle dependence of SdH frequencies obeys the $1/\cos\theta$ law, as shown in Fig. 3(c).

Those findings strongly evidence the following. This material fixed onto the PEN substrate under high pressure is a 2D massless Dirac fermion system. Although the chiral symmetry is broken (the Dirac cones are tilted), the Landau level structure is expressed as Eq. (1). Moreover, hole doping in this system is a success because the polarity of Hall resistance R_{xy} is positive in the magnetic field region in which SdH oscillations are observed [Fig. 3(a)].

B. Energy diagram of the present device

In this section, the distribution of doped hole density n_d in the layered direction is examined. The carrier density of each layer is estimated to be approximately 3.5×10^{13} cm^{-2} and 0.53×10^{13} cm^{-2} from the relationship $n_d = s4\pi B_f/\phi_0$, where $s = 4$ is the fourfold degeneracy and $\phi_0 = 4.14 \times 10^{-15}$ T m^2 is the flux quantum. When the Fermi velocity is approximately 3.5×10^4 m/s,[18] the Fermi energies $E_F/k_B = -\hbar v_F k_F = -\hbar v_F\sqrt{(n_d/s)/\pi}$ are located at approximately -41.8 and -8 K from the Dirac point, respectively. Regarding n_d of the first layer from an interface as the higher one (3.5×10^{13} cm^{-2}), Fig. 3(d) is the distribution of doped carrier density in the layered direction in this device.

This result should be compared with the solution of Poisson's equation. The doped carrier density $n(z)$ in a multilayered material is written by $n(z) \propto (L_n + L)^{-2}$ from Poisson's equation, where L_n is the number of layers from an interface and L is regarded as the number of effective layers (thickness).[19] The best fit of this equation with $L = 1$ indicates that the number of effective layers is unity.

Note that the detection of SdH oscillations with two frequencies indicates that the number of doped layers is more than two, but the doped densities after the second layers are much lower than that of the first layer. Thus, the second layer is in the quantum limit state (the state between $N = -1$ and 0 Landau levels, to be exact) at low magnetic fields, so that the SdH oscillations are observed only at magnetic fields below 1 T. Based on these findings, SdH signals at magnetic fields above 1 T are due to the Dirac particles of the first layer.

The lower limits of the carrier mobilities in the first and the second layers are roughly examined to be approximately 10^4 cm^2/V s and 3×10^4 cm^2/V s from the early SdH signals [$\omega_c\tau = (\mu B)^2 > 1$, respectively].

C. Quantum Hall states

Next, we discuss the quantum Hall state in the present device. Two obvious R_{xy} plateaus are observed at magnetic fields of approximately 3.5 and 5.5 T, which show R_{xx} minima [Fig. 3(a)]. In the previous section, we have demonstrated that the Landau level structure in the system with broken symmetry is expressed as Eq. (1). Based on conventional 2D Dirac fermion systems, we interpret the R_{xy} plateaus.

In this case, R_{xy} quantization is in accordance with $1/R_{xy} = \nu e^2/h$, where $\nu = \pm s(n + 1/2)$ with $s = 4$ is the quantized filling factor.[1,2] A conspicuous effect on the Dirac fermion system is that the factor of half-integer exists. Thus, probes of the quantum Hall plateaus for $|\nu| = 2, 6, 10, 14, \ldots$ are expected. In the data in Fig. 3(a), based on this step rule, $\nu_{\text{first}} = -6, -10, -14, -18$ for the first layer at R_{xy} plateaus or anomalies are required from SdH oscillations against the Landau index shown in Fig. 4.

The multilayered structure with a few hole-doped layers, however, gives rise to the lack of validity of the examination of ν from the values of the R_{xy} plateau. The values of the R_{xy} plateau depend on the thickness. On the other hand, R_{xx} is not zero but shows minima at R_{xy} plateaus. The thickness blurs the SdH oscillations and the quantum Hall plateau. In addition, we cannot ignore the sum of conductivities for the undoped

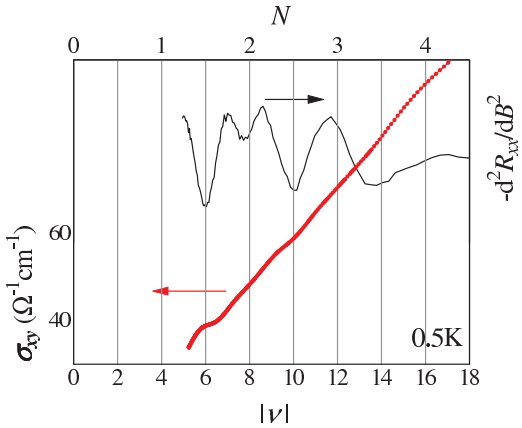

FIG. 4. (Color online) (a) Landau index N or filling factor for first layer $|\nu_{\rm first}|$ dependence of $-(d^2R_{xx}/dB^2)$ and σ_{xy}.

layers. For example, we can see this effect on R_{xy} at magnetic fields below 1.5 T. In this field region, the polarity of R_{xy} is negative and yet holes are injected, as shown in Fig. 3(a). This is a frequently observed behavior of the present material induced by doped electrons of ppm order that originate from unstable I_3^- anions.[6]

Let us examine whether the R_{xy} plateau regions in Fig. 3(a) are intrinsic quantum Hall states or not. Then, we will characterize the quantum Hall state of this system.

The following reasons convince us that at least the plateau region around 5.5 T is the complete quantum Hall state. This plateau appears between $N = -2$ and -1 Landau levels. The nonlocalized energy width for the $N = -2$ Landau level is roughly estimated to be approximately 7.2 K from the Landau level structure of Eq. (1) with $v_{\rm F} = 3.5 \times 10^4$ m/s in the nonplateau magnetic field region between 3.6 and 5.0 T. This value should be compared with the energy gap between $N = -2$ and -1 Landau levels, and is approximately 14 K at 5.5 T. Thus, the localized energy region to realize QHE is sufficient. The plateau region around 3.5 T, on the other hand, may not be the complete quantum Hall state. As nonlocalized energy widths for $N = -3$ and -2 Landau levels are close to the energy gap (approximately 9 K at 3.5 T) between $N = -3$ and -2 Landau levels, the localized energy region is very narrow.

The Hall conductivity $\sigma_{xy} = \rho_{xy}/(\rho_{xx}^2 + \rho_{xy}^2)$ will support those conclusions. We show a plot of σ_{xy} against the filling factor for the first layer in Fig. 4(a). The clear σ_{xy} plateau at $\nu_{\rm first} = -6$ (around 5.5 T) is the hallmark of the intrinsic QHE. Other σ_{xy} plateaus, however, are blurred.

The breakdown of the plateaus and resistance minima due to the high current intensity is also a characteristic feature of the QHE.[20–22] We verified that the plateaus and resistance minima were blurred with increasing current intensity, as shown in Fig. 5. Note that both of the data of R_{xy} and R_{xx} in the normal state are independent of the current intensity. In the quantum Hall state, Joule heat is locally generated near the current electrode at the sample edge. Nonequilibrium electron distribution generated at the sample edge gives rise to energy dissipation so that the breakdown of the QHE occurs.

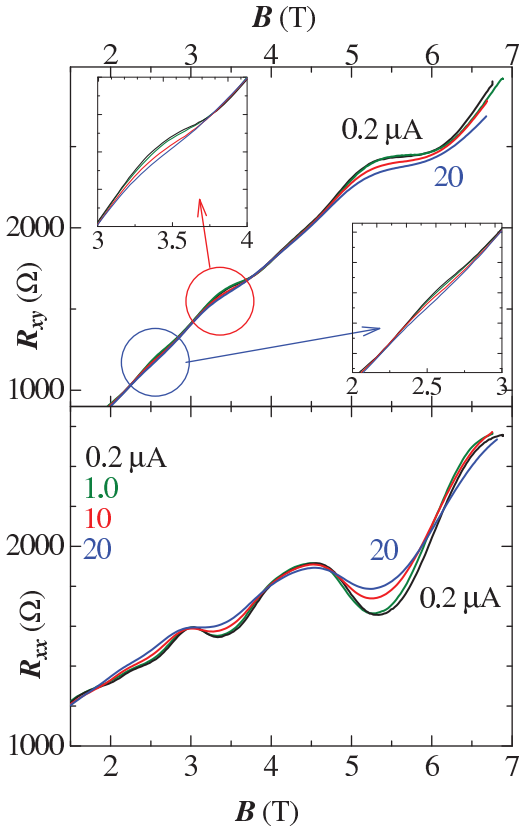

FIG. 5. (Color online) R_{xy} and R_{xx} for several current intensities at 0.5 K. The insets show R_{xy} of the regions from 2 to 3 T and from 3 to 4 T. The high intensities of the currents blur the plateaus and resistance minima.

D. Quantum Hall state around 5.5 T

In this section, we focus on the quantum Hall state around 5.5 T. The energy diagram shown in Fig. 6(a) is anticipated in the present device. For the first layer, $\nu_{\rm first} = -6$. As mentioned before, on the other hand, the Fermi energy (approximately 8 K from the Dirac point) at the second layer exists in the region between $N = -1$ and 0 Landau levels. Note that the spin-split energies $E_{\rm s} = \pm g\mu_{\rm B}B/2$ with $g = 2$ of zero mode are ± 3.6 K. In our experimental data for interlayer transport, however, $g = 1.1$ and therefore the spin-split energies are estimated to be ± 2.1 at 5.5 K. Thus, we expect the $\nu_{\rm second} = -2$ quantum Hall state for the second layer. Moreover, the $\nu_{\rm undoped} = 0$ quantum Hall state due to the spin splitting of zero mode is realized at the undoped layers. The total filling factor (Chern number) $\nu_{\rm total} = \nu_{\rm first} + \nu_{\rm second} + \Sigma\nu_{\rm undoped} = -6 - 2 + 0 = -8$ at 5.5 T should be prospected in the present device.

Note that as mentioned before, σ_{xx} and σ_{xy} for the undoped layers are not zero but finite low values. In this situation, it is difficult to examine the filling factor directly from the value of the σ_{xy} plateau. Hence, we investigate the sum of filling factors for the first and second layers from the thickness (number of layers L_n) dependence of R_{xx} and R_{xy}. Figures 6(b) and 6(c) show the L_n dependence of $\sigma_{xx}^{\rm sheet}L_n$ and $\sigma_{xy}^{\rm sheet}L_n$ calculated from R_{xx} and R_{xy} at 5.5 T where $\sigma_{xx}^{\rm sheet}$ and $\sigma_{xy}^{\rm sheet}$ are the averaged conductivity and the Hall conductivity per unit layer,

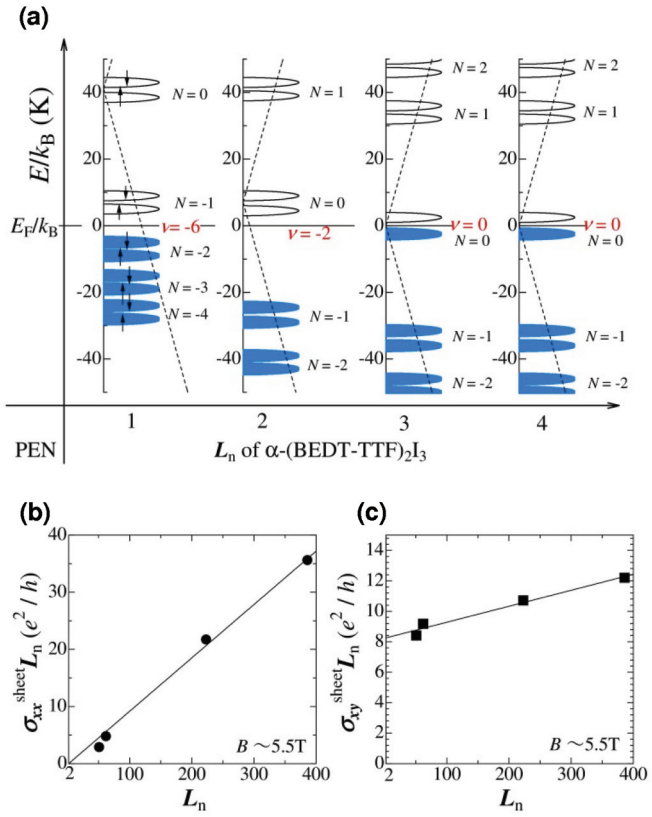

FIG. 6. (Color online) (a) Schematic energy diagram of the present device at 5.5 T. The Landau levels for the layers are drawn. The total filling factor (Chern number) $\nu_{total} = \nu_{first} + \nu_{second} + \Sigma\nu_{undoped} = -6 - 2 + 0 = -8$ is expected. (b) L_n dependence of $\sigma_{xx}^{sheet} L_n$. (c) L_n dependence of $\sigma_{xy}^{sheet} L_n$. Fitting lines indicate that $\sigma_{xx}^{sheet} L_n \sim 0$ and $\sigma_{xy}^{sheet} L_n \sim 8e^2/h$ at the limit of $L_n = 2$. Thus, the QHE with $\nu_{total} = -8$ is truly realized at the magnetic field of approximately 5.5 T.

respectively. We obtain $\sigma_{xx}^{sheet} L_n \sim 0$ and $\sigma_{xy}^{sheet} L_n \sim 8e^2/h$ at the limit of $L_n = 2$ from the fitting lines. Those results show that the QHE around 5.5 T is intrinsic and thus $\nu_{total} = -8$.

E. Conductivity of undoped layers

Lastly, we briefly discuss the conductivities for the undoped layers at the magnetic field of approximately 5.5 T. The slopes of the fitting lines in Figs. 6(b) and 6(c) give the conductivity and the Hall conductivity per unit layer of undoped layers, and those are approximately $0.07e^2/h$ and $0.008e^2/h$, respectively. Those values correspond well to the values of the crystals with no substrate.[9]

V. CONCLUSIONS

In conclusion, we provided crucial evidence that the energy of the Landau level in Dirac fermion systems with broken symmetry is the same as that in graphene. For this purpose, we performed hole doping of α-(BEDT-TTF)$_2$I$_3$ by fixing the thin crystal to a PEN substrate. This work demonstrates carrier injection effects on quantum transport phenomena in bulk Dirac fermion materials. The SdH signals with two frequencies whose phases were modified by Berry's phase π revealed the energy diagram of this device. Moreover, we characterized the multilayered QHE. The present device offers an ideal testing ground for a wider class of massless Dirac fermion systems. For example, we expect experimental studies of the helical surface state in multilayered massless Dirac fermion systems[23] and the Kosterlitz-Thouless transition (the broken valley symmetry) associated with tilted Dirac cones in high magnetic fields.[24]

ACKNOWLEDGMENTS

We thank T. Osada, A. Kobayashi, Y. Suzumura, T. Morinari, T. Tohyama, T. Kawarabayashi, and H. Fukuyama for valuable discussions. This work was partly supported by Grants-in-Aid for Scientific Research (No. 22224006, No. 23740270, and No. 25287089) from the Ministry of Education, Culture, Sports, Science and Technology, Japan and the Nanotechnology Platform Program (Molecule and Material Synthesis) of the Ministry of Education, Culture, Sports, Science and Technology (MEXT), Japan.

[1] K. S. Novoselov, A. K. Geim, S. V. Morozov, D. Jiang, M. I. Katsnelson, I. V. Grigorieva, S. V. Dubonos, and A. A. Firsov, Nature (London) **438**, 197 (2005).
[2] Y. Zhang, Y. W. Tan, H. Stormer, and P. Kim, Nature (London) **438**, 201 (2005).
[3] H. Kempa, P. Esquinazi, and Y. Kopelevich, Phys. Rev. B **65**, 241101(R) (2002).
[4] I. A. Luk'yanchuk and Y. Kopelevich, Phys. Rev. Lett. **93**, 166402 (2004).
[5] Y. Fuseya, M. Ogata, and H. Fukuyama, Phys. Rev. Lett. **102**, 066601 (2009).
[6] P. Richard, K. Nakayama, T. Sato, M. Neupane, Y.-M. Xu, J. H. Bowen, G. F. Chen, J. L. Luo, N. L. Wang, X. Dai, Z. Fang, H. Ding, and T. Takahashi, Phys. Rev. Lett. **104**, 137001 (2010).
[7] H. Zhang, C.-X. Liu, X.-L. Qi, X. Dai, Z. Fang, and S.-C. Zhang, Nat. Phys. **5**, 438 (2009).
[8] N. Tajima, M. Tamura, Y. Nishio, K. Kajita, and Y. Iye, J. Phys. Soc. Jpn. **69**, 543 (2000).
[9] N. Tajima, S. Sugawara, M. Tamura, R. Kato, Y. Nishio, and K. Kajita, J. Phys. Soc. Jpn. **75**, 051010 (2006).
[10] N. Tajima, S. Sugawara, M. Tamura, R. Kato, Y. Nishio, and K. Kajita, Europhys. Lett. **80**, 47002 (2007).
[11] N. Tajima, S. Sugawara, R. Kato, Y. Nishio, and K. Kajita, Phys. Rev. Lett. **102**, 176403 (2009).
[12] N. Tajima, R. Kato, S. Sugawara, Y. Nishio, and K. Kajita, Phys. Rev. B **85**, 033401 (2012).
[13] A. Kobayashi, S. Katayama, K. Noguchi, and Y. Suzumura, J. Phys. Soc. Jpn. **73**, 3135 (2004).

[14]S. Katayama, A. Kobayashi, and Y. Suzumura, J. Phys. Soc. Jpn. **75**, 054705 (2006).
[15]H. Kino and T. Miyazaki, J. Phys. Soc. Jpn. **75**, 034704 (2006).
[16]K. Bender, I. Hennig, D. Schweitzer, K. Dietz, H. Endres, and H. J. Keller, Mol. Cryst. Liq. Cryst. **108**, 359 (1984).
[17]T. Ando, J. Phys. Soc. Jpn. **74**, 777 (2005).
[18]N. Tajima, M. Sato, S. Sugawara, R. Kato, Y. Nishio, and K. Kajita, Phys. Rev. B **82**, 121420(R) (2010).
[19]G. Horowitz, M. E. Hajlaoui, and R. Hajlaoui, J. Appl. Phys. **87**, 4456 (2000).
[20]N. Q. Balaban, U. Meirav, H. Shtrikman, and Y. Levinson, Phys. Rev. Lett. **71**, 1443 (1993).
[21]S. Kawaji, K. Hirakawa, M. Nagata, T. Okamoto, T. Fukuse, and T. Gotoh, J. Phys. Soc. Jpn. **63**, 2303 (1994).
[22]A. Boisen, P. Bøggild, A. Kristensen, and P. E. Lindelof, Phys. Rev. B **50**, 1957 (1994).
[23]T. Osada, Phys. Status Solidi B **249**, 962 (2012).
[24]A. Kobayashi, Y. Suzumura, H. Fukuyama, and M. O. Goerbig, J. Phys. Soc. Jpn. **78**, 114711 (2009).